Bonding Between C2 and N2: A Localization-Induced σ Bond.

ARTICLE *in* JOURNAL OF THE AMERICAN CHEMICAL SOCIETY · DECEMBER 1990

Impact Factor: 12.11 · DOI: 10.1021/ja00182a006

Bonding between C_2 and N_2: A Localization-Induced σ Bond

M. K. Scheller,† L. S. Cederbaum,*,† and F. Tarantelli‡

Contribution from the Theoretische Chemie, Physikalisch-Chemisches Institut, Universität Heidelberg, Im Neuenheimer Feld 253, D-6900 Heidelberg, Federal Republic of Germany, and Dipartimento di Chimica, Università di Perugia, I-06100 Perugia, Italy. *Received April 19, 1990*

Abstract: Calculations on the experimentally and theoretically unknown molecule CCNN are presented comprising geometry optimization, potential energy surface, and electric dipole moment computations. At the Hartree–Fock level, the results predict that CCNN has a $^1\Sigma^+$ closed-shell ground state and a linear equilibrium geometry. Moreover, at this level of theory the molecule is found to be remarkably stable against unimolecular dissociation into the constituent monomers $C_2(^1\Sigma_g^+)$ and $N_2(^1\Sigma_g^+)$. The dissociation path exhibits an energy barrier. A theoretical analysis of the Hartree–Fock electronic structure shows that localization of the charge density controls the bonding, revealing a new type of binding mechanism. This picture is supported by the results of configuration interaction calculations that confirm the existence of an energy barrier to dissociation. The strong correlation effects found in the dissociation products call for a more complete treatment and do not allow yet a definitive statement about whether the molecule CCNN is stable or just metastable.

I. Introduction

Much attention has been paid in the literature to dimers and van der Waals systems (clusters) made up of a single type of monomer (see ref 1 for a limited number of examples). Probably because of the greater complexity, corresponding systems built up of different molecules have been studied to a much lesser extent.

This tendency is also obvious from inspection of the series of molecules with empirical formula C_2N_2. Cyanogen (**1**, NCCN), isocyanogen (**2**, CNCN), and diisocyanogen (**3**, CNNC), the (formal) dimers of the cyano radical (CN), are theoretically well-analyzed systems.[2] The species **1** and **2** are also accessible by synthesis.[3] We refer to these molecules as homodimers, expressing that only a single type of monomer (CN) is present.

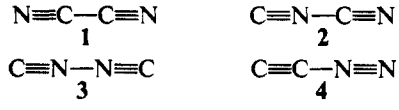

As far as it is known to us, the last possible molecule of empirical formula C_2N_2, diaza-dicarbon (**4**, CCNN), remained up to now completely untreated both theoretically and experimentally. This may be rationalized considering that CCNN must be seen as constituted by the unlike closed-shell monomers $C_2(^1\Sigma_g^+)$ and $N_2(^1\Sigma_g^+)$. Without consideration of van der Waals forces, the physical and chemical expectation about two closed-shell systems approaching each other is that they repel. Therefore, at a first glance, CCNN may intuitively be expected to be an overall unstable species. This would explain the lack of attention paid to this molecular system.

Following our studies on the homodimers **1**–**3**[2] we theoretically analyzed CCNN to complete our treatment of the C_2N_2 isomers. At Hartree–Fock level of theory, we were very surprised to find that CCNN is remarkably stable against dissociation into the constituent closed-shell monomers $C_2(^1\Sigma_g^+)$ and $N_2(^1\Sigma_g^+)$. The binding energy of 3.0 eV and the appearance of an energy barrier (3.2 eV of activation energy) to dissociation (both values after correction of the basis set superposition error) clearly excluded the characterization of CCNN as a van der Waals molecule and revealed instead that $C_2(^1\Sigma_g^+)$ and $N_2(^1\Sigma_g^+)$ are held together by chemical bonding as in "normal" molecules. Analyzing the Hartree–Fock electronic structure of CCNN in the $^1\Sigma^+$ closed-shell ground state, we attributed the observed stability to a strong σ bond connecting the closed-shell monomers $C_2(^1\Sigma_g^+)$ and $N_2(^1\Sigma_g^+)$. This chemical bonding is controlled by strong spatial localizations of the charge density and reveals a new type of binding mechanism, which is introduced as "localizing hybridization" in this work.

The classification of CCNN as a normal molecule is supported by configuration interaction computations. These methods confirm the existence of an energy barrier to dissociation. But according to strong electron correlation effects found in the dissociation products (especially in $C_2(^1\Sigma_g^+)$), we are not yet able to give a definitive statement about whether the molecule CCNN is (absolutely) stable or just metastable to unimolecular dissociation into the closed-shell monomers $C_2(^1\Sigma_g^+)$ and $N_2(^1\Sigma_g^+)$.

II. Geometry and Potential Energy Surface at the HF Level

Geometry. The Hartree–Fock (HF) results presented here were obtained with a double-ζ plus polarization (DZP) basis set of primitive Gaussian-type functions with Dunning's (9s5p1d) → (4s2p1d) contraction.[4] Exponents for the d-polarization functions were 0.72 and 0.98 for C and N, respectively.[5] Thus, the DZP basis set comprises a total of 64 contracted Gaussian-type functions.

Our first aim has been to assess the equilibrium structure of CCNN in its electronic ground state. Geometry optimization computations were performed in the point-group symmetries C_s, C_{2v}, C_{2h}, and $C_{\infty v}$ with conventional restricted self-consistent field (SCF) methods.[6]

† Universität Heidelberg.
‡ Università di Perugia.

(1) van der Waals Systems. *Top. Curr. Chem.* **1980**, *93*. Margenau, H.; Kestner, N. R. *Theory of Intermolecular Forces*; Pergamon: Elmsford, NY, 1971. Wasintynski, T.; van der Avoird, A.; Berns, R. M. *J. Chem. Phys.* **1978**, *69*, 5288. Mulder, F.; van Dijk, G.; van der Avoird, A. *Mol. Phys.* **1980**, *39*, 407. Kofranetz, M.; Lischka, H.; Karpfen, A. *Mol. Phys.* **1987**, *61*, 1519. Slanina, Z. *Chem. Phys. Lett.* **1987**, *142*, 512. Hiraoka, K.; Yamabe, S. *Chem. Phys. Lett.* **1989**, *154*, 139.

(2) Milligan, D. E.; Jacox, M. E. *J. Chem. Phys.* **1967**, *47*, 278. Cederbaum, L. S.; Domcke, W.; von Niessen, W. *Chem. Phys.* **1975**, *10*, 459. Haese, N. N.; Woods, R. C. *J. Chem. Phys.* **1980**, *73*, 4521. Sana, M.; Leroy, L. *J. Mol. Struct.* **1981**, *76*, 259. von Niessen, W.; Cederbaum, L. S.; Schirmer, J.; Diercksen, G. H. F.; Kraemer, W. P. *J. Electron Spectrosc. Relat. Phenom.* **1982**, *28*, 45. Nguyen, M. T. *Chem. Phys. Lett.* **1989**, *157*, 430. Botschwina, P.; Sebald, P. *Chem. Phys.*, to be published. Cederbaum, L. S.; Tarantelli, F.; Weikert, H.-G.; Scheller, M. K.; Köppel, H. *Angew. Chem.* **1989**, *101*, 770. Scheller, M. K.; Weikert, H. G.; Cederbaum, L. S.; Tarantelli, F. *J. Electron Spectros. Relat. Phenom.* **1990**, *51*, 75. Scheller, M. K. Thesis, Universität Heidelberg, Germany, 1989.

(3) Gay-Lussac, L. J. *Ann. Chim. (Paris)* **1815**, *95*, 172. Maki, A. G. *J. Chem. Phys.* **1965**, *43*, 3193. van der Does, T.; Bickelhaupt, F. *Angew. Chem.* **1988**, *100*, 998. Stroh, F.; Winnewisser, M. *Chem. Phys. Lett.* **1989**, *155*, 21. Grabant, O.; de Lange, C. A.; Mooyman, R.; van der Does, T.; Bickelhaupt, F. *Chem. Phys. Lett.* **1989**, *155*, 221. Yamada, K. M. T.; Markus, M. W.; Jontgen, W.; Kock, R.; Vogel, E.; Altenbach, H.-T. *Chem. Phys. Lett.* **1989**, *160*, 113. Stroh, F.; Winnewisser, B. P.; Winnewisser, M.; Reisenauer, H. P.; Maier, G.; Goede, S. J.; Bickelhaupt, F. *Chem. Phys. Lett.* **1989**, *160*, 105.

(4) Dunning, T. H., Jr. *J. Chem. Phys.* **1971**, *55*, 716.

(5) Ahlrichs, R.; Taylor, P. R. *J. Chim. Phys. Phys.-Chim. Biol.* **1981**, *78*, 315.

(6) Guest, M. F.; Kendrick, J. *GAMESS*; Comp. Science Group, Science and Engineering Research Council, Daresbury Laboratory: Daresbury, Warrington, WA4 4AD. Schaefer, H. F. *The Electronic Structure of Atoms and Molecules*; Addison-Wesley: Menlo Park, 1972.

0002-7863/90/1512-9484$02.50/0

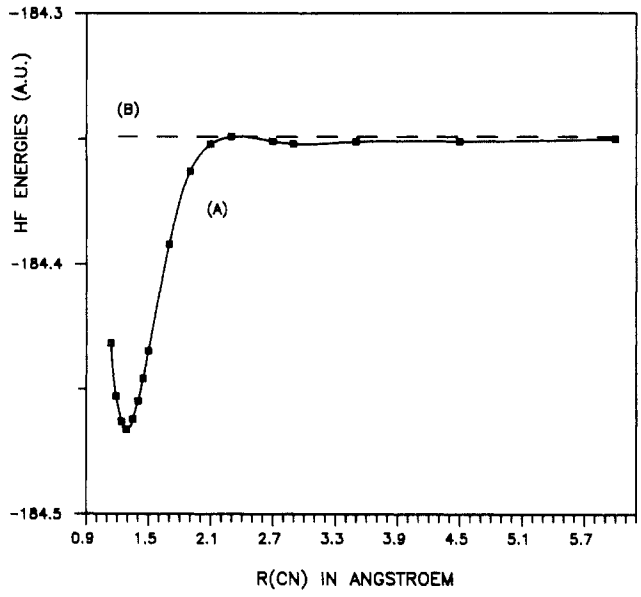

Figure 1. Potential energy surface (curve A) of $CCNN(^1\Sigma^+)$ computed at HF level. Line B denotes the total HF energy of $C_2(^1\Sigma_g^+)$ and $N_2(^1\Sigma_g^+)$ at their experimental geometries. Energies were obtained with the DZP basis.

The following linear equilibrium structure of point-group symmetry $C_{\infty v}$ was obtained for CCNN in the electronic closed-shell ground state $^1\Sigma^+$:

$$C\overset{1.248\ \text{Å}}{\text{---}}C\overset{1.288\ \text{Å}}{\text{---}}N\overset{1.109\ \text{Å}}{\text{---}}N$$

A linear structure in the closed-shell ground state was also found for the homodimers of empirical formula C_2N_2.[2]

Compared with the average interstice between the molecules (or atoms) constituting van der Waals complexes,[1] the narrow distance between the $C_2(^1\Sigma_g^+)$ and $N_2(^1\Sigma_g^+)$ subgroups of CCNN (R_{CN} = 1.288 Å) strongly favors the classification of this molecule as a chemical bonding system rather than as held together by weak van der Waals forces. With respect to the experimental bond distances of the CN radical (1.177 Å[7]) and of the molecules C_2 (1.243 Å[8]) and N_2 (1.095 Å[9]), the central CN bond of CCNN is strongly lengthened while both terminal CC and NN bonds are only slightly enlarged.

These results manifest that it is reasonable to look upon the CCNN system as build up by the chemical bonding of the closed-shell monomers $C_2(^1\Sigma_g^+)$ and $N_2(^1\Sigma_g^+)$. We will classify the CCNN system as a codimer, meaning that two unlike monomer types (C_2 and N_2) are present in this molecule.

The electron distribution in the $^1\Sigma^+$ ground state of CCNN may be rationalized considering the following valence structure:

$$|\bar{C}{\equiv}C{-}N^+{\equiv}N|$$

As will be seen in the course of this work, this structure is completely satisfactory to describe the molecular properties of $CCNN(^1\Sigma^+)$. In particular, no additional valence structure must be included to explain the partial double-bond character of the central CN bond and the slight lengthening of both terminal bonds. These phenomena are inherently implied in molecules where conjugated triple bonds are present.[10]

Potential Energy Surface. The dissociation path of $CCNN(^1\Sigma^+)$ leading to the separated $C_2(^1\Sigma_g^+)$ and $N_2(^1\Sigma_g^+)$ molecules was computed by fixing the central CN bond at various values and by optimizing each time the terminal CC and NN bond lengths in $C_{\infty v}$ symmetry. Curve A in Figure 1 presents the energy data obtained. Line B, which is referred to as the asymptotic limit, denotes the total HF energy of the separated monomers $C_2(^1\Sigma_g^+)$ and $N_2(^1\Sigma_g^+)$ at their experimental geometries.[8,9]

From the figure, it can immediately be seen that our statements on the high stability of CCNN to unimolecular dissociation and on the chemical bonding of $C_2(^1\Sigma_g^+)$ and $N_2(^1\Sigma_g^+)$ are correct. The dissociation energy, D_e (difference between the asymptotic limit and the minimum of curve A), is given by 3.22 eV. In comparison with the energy surfaces of the C_2N_2 homodimers,[11] that of $CCNN(^1\Sigma^+)$ is very steep along R_{CN} for distances less than 2.3 Å. This is reflected by the narrow gap of about only 1 Å between the minimum and dissociation limit (R_{CN} > 2.3 Å).

Beyond R_{CN} = 2.3 Å, curve A describes a second but very flat (local) minimum of the total HF energy. This phenomenon is probably an artifact of the HF model used in conjunction with the truncated, i.e., incomplete and unbalanced, DZP basis set. A correction was obtained by computing the so-called basis set superposition error (BSSE),[12] which represents the energy lowering of each monomer ($C_2(^1\Sigma_g^+)$ or $N_2(^1\Sigma_g^+)$) upon addition of basis functions localized on the other monomer ($N_2(^1\Sigma_g^+)$ or $C_2(^1\Sigma_g^+)$). The procedure invoked to compute the BSSE has been theoretically justified,[13] and it appears to work numerically reasonably well[14] if the atomic basis sets are not too badly chosen.

Due to the correction of the BSSE, the potential energy surface of $CCNN(^1\Sigma^+)$ is shifted toward more positive energies. This reduces D_e to 3.0 eV, and in particular the (local) flat energy minimum vanishes. Furthermore, the dissociation path is now found to exhibit an energy barrier E_A^* to dissociation. The barrier is defined as the energy difference between the (local) maximum and the (unique) minimum of the corrected energy surface. E_A^* was computed to be 3.2 eV, expressing that the top of the barrier is 0.2 eV more positive in energy than line B.

Due to the existence of an energy barrier, the potential energy surface describes a repulsive interaction between $C_2(^1\Sigma_g^+)$ and $N_2(^1\Sigma_g^+)$ at R_{CN} larger than 2.3 Å. Without consideration of van der Waals forces, this repulsion is in agreement with the common expectation relative to two closed-shell systems approaching each other. In the case of $C_2(^1\Sigma_g^+)$ and $N_2(^1\Sigma_g^+)$, the Coulombian repulsions of the high negative charge densities, which are present at the terminal outsides of both linearly approaching closed-shell monomers, may participate in this repulsive interaction. In the next section, we will analyze what kind of changes of the molecular properties of the closed-shell monomers must take place to imply the course of curve A for R_{CN} less than 2.3 Å.

III. Discussion: Localization-Induced σ Bond

To understand what kind of molecular phenomena are responsible for the building up of a chemical bonding interaction between $C_2(^1\Sigma_g^+)$ and $N_2(^1\Sigma_g^+)$, we computed the charge density distribution of the individual $CCNN(^1\Sigma^+)$ molecular orbitals (MOs) at the HF equilibrium geometry. The data concerning the 9σ, 8σ, and 6σ MOs are illustrated in Figure 2a–c, respectively. Results for the remaining $CCNN(^1\Sigma^+)$ MOs are not given since they are not necessary for the following discussions and explanations.

The 9σ MO (Figure 2a) is almost completely located on and bonding between the atomic units of the C_2 monomer. Correspondingly, the 8σ MO (Figure 2b) is in the most part centered at the atoms of the N_2 group. The strong spatial localization of the charge density, evidently expressed by the shape of both σ MOs, is a direct consequence of the process of stable chemical bonding between $C_2(^1\Sigma_g^+)$ and $N_2(^1\Sigma_g^+)$. This is obvious by recalling that the homonuclear molecules $C_2(^1\Sigma_g^+)$ and $N_2(^1\Sigma_g^+)$ do only cover centrosymmetrical and delocalized spatial MOs.

Due to the localization of the charge density at the C and N outsides of $CCNN(^1\Sigma^+)$, the 9σ and 8σ MOs are referred to as lone pairs of electrons or lone orbitals. Furthermore, these MOs

(7) Sutton, L. E., Ed. *Spec. Publ.-Chem. Soc.* **1965**, *18*.
(8) Ballik, E. A.; Ramsay, D. A. *Astrophys. J.* **1963**, *137*, 61, 84.
(9) Krummacher, S.; Schmidt, V.; Wuilleumier, F. *J. Phys. B* **1980**, *13*, 3993.
(10) Politzer, P.; Kasten, S. D. *J. Phys. Chem.* **1976**, *80*, 283 and references therein.
(11) Scheller, M. K.; Cederbaum, L. S.; Tarantelli, F. Unpublished results.
(12) Wormer, P. E. S.; van der Avoird, A. *J. Chem. Phys.* **1975**, *62*, 3326. Kestner, N. R. *J. Chem. Phys.* **1968**, *48*, 252.
(13) Boys, S. F.; Bernardi, F. *Mol. Phys.* **1970**, *19*, 553.
(14) Balski, M.; Chalasinski, G. *Theor. Chim. Acta* **1977**, *44*, 399.

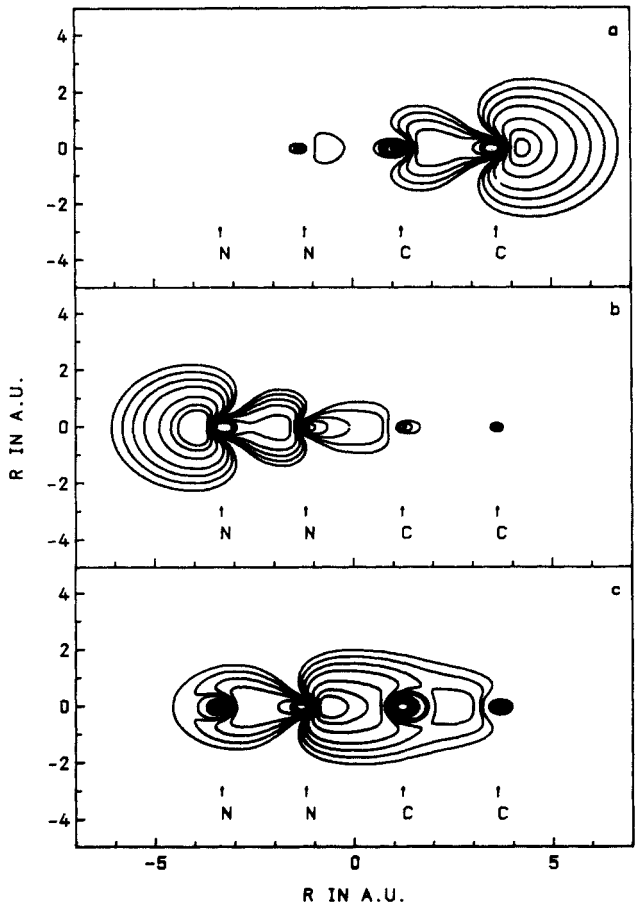

Figure 2. Calculated charge density distribution of the 9σ (a), 8σ (b), and 6σ MOs (c) of $CCNN(^1\Sigma^+)$. Data were obtained at the HF equilibrium geometry with the DZP basis set.

are the only ones found to be localized at the terminal outsides of CCNN. This justifies our exclusive consideration of the valence structure given in section II. The location of the negative center of partial charge may then be rationalized as a consequence of the spatial localization of the charge density at the 9σ MO.

The shape of the delocalized 6σ MO (Figure 2c) evidently expresses that this orbital is bonding at both terminal CC and NN units as well as in the region between them. According to our data, it is the 6σ MO that covers the central and most stable σ bond $CCNN(^1\Sigma^+)$ connecting the $C_2(^1\Sigma_g^+)$ and $N_2(^1\Sigma_g^+)$ monomers. The results evidently express that normal chemical bonding rather than formation of a van der Waals complex takes place between the closed-shell molecules $C_2(^1\Sigma_g^+)$ and $N_2(^1\Sigma_g^+)$.

Up to now, we analyzed the behavior of the charge density at the HF equilibrium geometry of $CCNN(^1\Sigma^+)$. To investigate how the above-mentioned phenomena develop by progressive interaction of $C_2(^1\Sigma_g^+)$ and $N_2(^1\Sigma_g^+)$, we employed a Mulliken population analysis.[15] The analysis was performed with the optimized HF structures already employed to compute the potential energy surface (curve A in Figure 1). Parts a–c of Figure 3 illustrate the data obtained for the 9σ, 8σ, and 6σ MOs of $CCNN(^1\Sigma^+)$, respectively.

As is indicated by the results at $R_{CN} = 3.5$ Å, the 9σ and 6σ MOs originate from delocalized orbitals of the $C_2(^1\Sigma_g^+)$ monomer. The 8σ MO is derived from a delocalized MO of the $N_2(^1\Sigma_g^+)$ molecule. As $C_2(^1\Sigma_g^+)$ and $N_2(^1\Sigma_g^+)$ approach each other along the R_{CN} coordinate ($R_{CN} \geq 2.3$ Å), a remarkable and continuously increasing spatial localization of the charge density is visible at the 9σ and 8σ MOs. However, the 6σ MO remains almost perfectly delocalized in character.

(15) Cook, D. B. *Ab Initio Valence Calculations in Chemistry*; Butterworths: Stoneham, MA, 1974. Mulliken, R. S. *J. Chem. Phys.* **1955**, *23*, 1833, 1841.

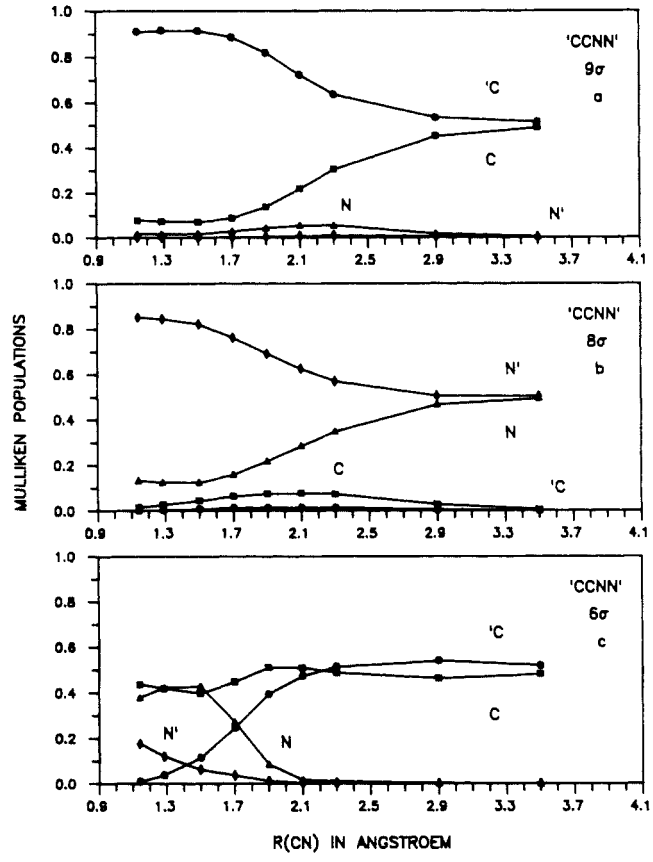

Figure 3. Results from the Mulliken population analysis of the 9σ (a), 8σ (b), and 6σ MOs (c) of $CCNN(^1\Sigma^+)$. Data were obtained at the optimized HF geometries with the DZP basis set.

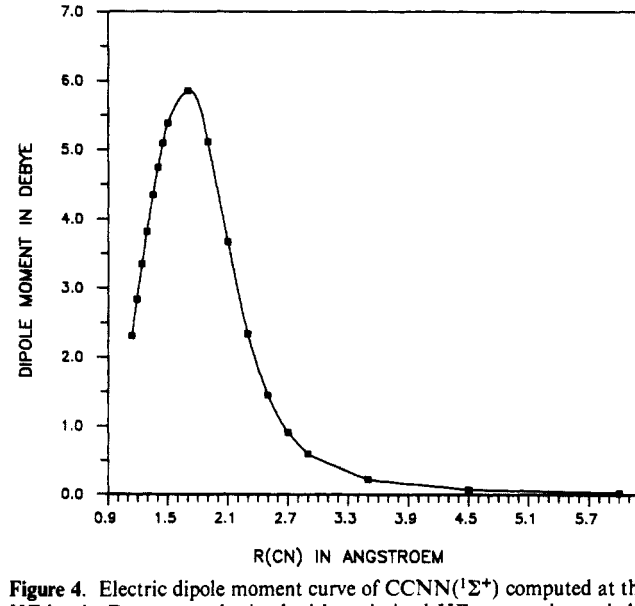

Figure 4. Electric dipole moment curve of $CCNN(^1\Sigma^+)$ computed at the HF level. Data were obtained with optimized HF geometries and the DZP basis set.

At R_{CN} less than 2.3 Å, a rapid localization of the 9σ and 8σ orbitals and the simultaneous formation of the central CN bond (6σ MO) are observed. The process ends at $R_{CN} \approx 1.5$–1.6 Å. Compared with the results on the potential energy surface (curve A in Figure 1), these findings unequivocally reveal that the enhancement in stability by bonding between $C_2(^1\Sigma_g^+)$ and $N_2(^1\Sigma_g^+)$ is closely associated with the strong development of spatial charge density localization.

Before analyzing the origin of the behavior of the spatial charge distribution, we now present the electric dipole moment curve of $CCNN(^1\Sigma^+)$. The results illustrated in Figure 4 were obtained

Table I. Contributions of the C_2 and N_2 MOs to the MOs of CCNN Obtained at the HF Equilibrium Geometry[a,b]

CCNN	5σ	6σ	7σ	8σ	1π	9σ	2π	10σ
ϵ_i(au)	−1.560	−1.186	−0.973	−0.746	−0.736	−0.462	−0.409	+0.243 (−0.070)
$C_2(2\sigma_g)$	0.002	−0.464*	0.809	0.041		0.076		1.297 (0.006)
$C_2(2\sigma_u)$	0.010	0.268	0.262	−0.202		0.709*		−1.721 (0.153)
$C_2(1\pi_u)$					−0.185		0.905*	
$C_2(3\sigma_g)$	−0.013	−0.172	−0.272	0.138		0.680		1.493* (−0.968)
$N_2(2\sigma_g)$	−1.000*	0.254	0.068	−0.081		0.002		−1.651 (−0.038)
$N_2(2\sigma_u)$	−0.117	−0.483	−0.233*	−0.724		0.020		−1.305 (0.180)
$N_2(3\sigma_g)$	−0.081	−0.311	−0.073	0.671*		0.059		−1.327 (−0.222)
$N_2(1\pi_u)$					−0.937*		−0.395	

[a] Numbers in parentheses refer to an R_{CN} of 2.3 Å. [b] The asterisk denotes the monomer MOs to which the CCNN MOs develop at dissociation.

with use of the HF structures already used to compute the energy surface (curve A in Figure 1). The very peculiar shape of the dipole moment curve can now be explained and understood with the results obtained from the analysis of the charge density aggregations as background information.

The asymptotic increase of the dipole moment when $C_2(^1\Sigma_g^+)$ and $N_2(^1\Sigma_g^+)$ interact repulsively ($R_{CN} \geq 2.3$ Å) is in the most part due to the beginning charge density localization at the 9σ and 8σ MOs. Other effects (like penetration, induction, dispersion, etc.) should be of subordinate importance to explain the dipole moment value of 2.33 D computed at $R_{CN} = 2.3$ Å.

The region of linear-increasing dipole moment between $R_{CN} = 2.3$ and 1.9 Å indicates that the centers of partial charge must be separated by the central CN bond of $CCNN(^1\Sigma^+)$. This fact was already predicted by the valence structure given in section II. Furthermore, it is evident that the reduction of the dipole moment due to the shortening of R_{CN} (decrease of the separation between the centers of partial charge) must by far be overcompensated by the increase of the spatial aggregation of the charge density. The latter obviously results in a tremendous concentration of charge at the locations of the partial charge centers. For example, at $R_{CN} = 1.7$ Å, where the dipole moment exhibits a maximal value of 5.85 D, each of the centers of positive and negative partial charge, located approximately at the central N and terminal C atoms, respectively, is associated with about 0.8 unit of charge.

At the left side of the dipole moment maximum, the decrease of the dipole moment due to the shortening of R_{CN} dominates the course of the curve. This result reflects our statement (Figure 3) that the spatial charge density aggregation is complete at an R_{CN} between about 1.5 and 1.6 Å. At the HF equilibrium structure, we computed a remarkable dipole moment value of 3.44 D.

To complete the discussion of the dipole moment, it is interesting to note that the computed value remains essentially unaltered upon inclusion of electron correlation: We obtain 3.49 D at SDCI, 3.15 D at MCPF, and 3.0–3.1 D at MRCI level of theory. The calculations were done with the DZP basis. Further comments upon these theoretical methods and their application in this work are given in section IV. The large dipole moment calculated for $CCNN(^1\Sigma^+)$ visualizes the intensity of charge aggregation that occurs upon interaction between the homonuclear and thus unpolar closed-shell systems $C_2(^1\Sigma_g^+)$ and $N_2(^1\Sigma_g^+)$.

Our intention is now to discuss and clarify the origin of the spatial charge density aggregations that appear in connection with the chemical bonding between $C_2(^1\Sigma_g^+)$ and $N_2(^1\Sigma_g^+)$. Our analysis is based on data obtained by computing the contributions of the $C_2(^1\Sigma_g^+)$ and $N_2(^1\Sigma_g^+)$ MOs to the MOs of $CCNN(^1\Sigma^+)$. Table I summarizes our results obtained at the HF equilibrium geometry. The numbers in parentheses were computed for the virtual 10σ MO of CCNN with use of the HF geometry: $R_{CC} = 1.253$ Å; $R_{CN} = 2.3$ Å: $R_{NN} = 1.075$ Å. The asterisk denotes everywhere the monomer MO to which the appropriate CCNN MO develops at dissociation. In addition, a row including the HF orbital energies ϵ_i of the $CCNN(^1\Sigma^+)$ MOs is given in the table.

In Table I, the underlined numbers guide us to classify the spatially localized 9σ and 8σ MOs as almost pure linear combinations (LCs) of the $2\sigma_u$ and $3\sigma_g$ orbitals of $C_2(^1\Sigma_g^+)$ and $N_2(^1\Sigma_g^+)$, respectively. The linearly combined monomer MOs contribute to almost the same extent to both CCNN MOs. As is symbolized by the asterisk, the 9σ MO develops at dissociation to the $C_2(2\sigma_u)$ orbital while the 8σ MO becomes the $N_2(3\sigma_g)$ orbital.

To clarify the charge density localization at the 9σ and 8σ MOs, it is extremely important to note that the constituting linearly combined monomer MOs are of different parity, "g" and "u", respectively. It is this difference in the symmetry of the $2\sigma_u$ and $3\sigma_g$ MOs that causes the localization of each of the two LCs (sum and difference) at one atomic site of the monomer species. This scheme simply explains the spatial charge density localization at CCNN, and we will refer to it as "localizing hybridization". The LCs formed are then referred to as "localized hybrids".

The above discussion clarifies the sudden change in electronic structure occurring as $C_2(^1\Sigma_g^+)$ and $N_2(^1\Sigma_g^+)$ approach each other along a linear path. It is interesting to mention here that a comparable drastic change in the bonding mechanism has been theoretically described for the open-shell dimer $(CO)_2^+$,[16] where the approaching CO and CO^+ units go over a barrier separating a weak CC bond structure and a strong CC bond situation. Different from the present case, however, the two electronic structures in $OCCO^+$ correspond to crossing states of different symmetry along the linear path, and it is only through bending (to a trans C_{2h} structure) that the two states couple and give rise to an avoided crossing. It is interesting to note that the weak CC bond at longer distance is due to the presence of the unpaired σ electron of CO^+. In $CCNN(^1\Sigma^+)$, the $C_2(^1\Sigma_g^+)$ and $N_2(^1\Sigma_g^+)$ molecules approach on a closed-shell surface, and the long-range part of the curve is, therefore, repulsive. The bonding mechanism in $CCNN(^1\Sigma^+)$ involves a $\sigma \rightarrow \sigma^*$ excitation in C_2, whereas in $(CO)_2^+$ the transition between the two bonding structures involves essentially a $\sigma \rightarrow \pi^*$ excitation in CO. The remarkable novelty exhibited by CCNN is that both C_2 and N_2 are closed-shell molecules and their bonding is accompanied by an enormous charge transfer to the terminal C atom, leading to the unusually large dipole moment.

It is now important to discuss some theoretical features of the localizing hybridization scheme. Let us begin with the $N_2(^1\Sigma_g^+)$ molecule. The $2\sigma_u$ and $3\sigma_g$ MOs of this system are both doubly occupied. Therefore, the mechanism of localizing hybridization corresponds to a simple linear transformation in the occupied orbital space. In this case, the total energies of the delocalized and localized systems are identical. To a first approximation, the energy of the localized hybrids is simply given as the arithmetical mean of the orbital energies of the linearly combined MOs of $N_2(^1\Sigma_g^+)$.

Turning to the $C_2(^1\Sigma_g^+)$ molecule, we note that the $3\sigma_g$ MO is *not occupied*. The localizing hybridization now involves both the occupied and the virtual orbital spaces. This necessarily implies a rise in the total energy of the localized system with respect to the energy of the original delocalized system. We refer to this difference in the total energy as "localization energy" (E_{LOC}).

(16) Blair, J. T.; Weisshaar, J. C.; Carpenter, J. E.; Weinhold, F. *J. Chem. Phys.* **1987**, *87*, 392. Blair, J. T.; Weisshaar, J. C.; Weinhold, F. *J. Chem. Phys.* **1988**, *88*, 1467.

The quantity E_{LOC} can be derived from the expression for the total HF energy of the delocalized molecular system:

$$E_0 = 2\sum_{i\in} h_{ii} + \sum_{i,j\in} 2J_{ij} - K_{ij} \quad (1)$$

The indices i and j label MOs belonging to the occupied orbital space (symbolized by $\in$). The quantities h_{ii}, J_{ij}, and K_{ij} denote conventional matrix elements of the one-particle operator, Coulomb and exchange integrals, respectively. Identifying the occupied $2\sigma_u$ MO of $C_2(^1\Sigma_g^+)$ with φ_a ($a\in$) and the unoccupied $3\sigma_g$ MO with φ_b ($b\notin$), we introduce the hybrids formed by linear combinations of φ_a and φ_b

$$\phi_\pm = \frac{1}{2^{1/2}}(\varphi_a \pm \varphi_b) \quad (2)$$

with

$$\langle\phi_\pm|\phi_\pm\rangle = 1 \qquad \langle\phi_\pm|\phi_\mp\rangle = 0 \quad (3)$$

Replacing φ_a in eq 1 by $\phi_\pm$ yields the following expression

$$E_\pm = 2\sum_{i\in;i\neq a} h_{ii} + 2h_{\pm\pm} + \sum_{\substack{ij\in\\ij\neq a}} (2J_{ij} - K_{ij}) + 2\sum_{i\neq a}(2J_{i\pm} - K_{i\pm}) + J_{\pm\pm} \quad (4)$$

$E_\pm$ denotes the total energy of the hybridized system. Due to this replacement, the summations in eq 4 exclude the occupied index a. Noting the different symmetry of the $2\sigma_u$ and $3\sigma_g$ MOs, we obtain:

$$E_{LOC} = E_\pm - E_0 = h_{bb} - h_{aa} + \sum_{i\in}[2(J_{ib} - J_{ia}) - (K_{ib} - K_{ia})] - 2J_{ab} + K_{ab} + J_{\pm\pm} \quad (5)$$

This equation defines the localization energy E_{LOC} as the difference of the total HF energy of the localized ($E_\pm$) and delocalized (E_0) systems. Introducing the orbital energies ϵ_a and ϵ_b yields a more simple expression:

$$E_{LOC} = \epsilon_b - \epsilon_a - (2J_{ab} - K_{ab}) + J_{\pm\pm} \qquad \epsilon_b > \epsilon_a \quad (6)$$

The term in parentheses and $J_{\pm\pm}$ are always positive. According to the sign, the first represents a gain in the total HF energy (attraction) due to localizing hybridization while the latter represents a loss in the energy (repulsion). Using the term

$$J_{\pm\pm} = \tfrac{1}{4}(J_{aa} + J_{bb} + 2J_{ab} + 4K_{ab}) \quad (7)$$

to substitute $J_{\pm\pm}$ in eq 6 yields the final expression for E_{LOC}:

$$E_{LOC} = \epsilon_b - \epsilon_a + \tfrac{1}{4}(J_{aa} + J_{bb}) - \tfrac{3}{2}J_{ab} + 2K_{ab} \quad (8)$$

With use of eq 8, the value of E_{LOC} due to localizing hybridization of the $C_2(^1\Sigma_g^+)$ molecule was computed to be +0.272 au (+7.410 eV).

The virtual character of the $C_2(3\sigma_g)$MO also implies that the "orbital" energy $\epsilon_\pm$ of the localized hybrids is not simply given as the arithmetical mean of the HF orbital energies of the linearly combined MOs. Starting with the expression for the HF orbital energy ϵ_a of the occupied MO φ_a (the $C_2(2\sigma_u)$ MO in the present case)

$$\epsilon_a = h_{aa} + \sum_{i=1}^{N}(2J_{ia} - K_{ia}) \quad (9)$$

and replacing φ_a by $\phi_\pm$ on the rhs of this equation yields the following expression for $\epsilon_\pm$:

$$\epsilon_\pm = \tfrac{1}{2}(h_{aa} + h_{bb}) + \sum_{i\neq a}(2J_{i\pm} - K_{i\pm}) + J_{\pm\pm} \quad (10)$$

Using eq 7, we obtain the final result for the orbital energy of the localized hybrids:

$$\epsilon_\pm = \tfrac{1}{2}(\epsilon_a + \epsilon_b) - \tfrac{1}{4}(J_{aa} - J_{bb} + 2J_{ab} - 6K_{ab}) \quad (11)$$

Equation 11 shows clearly the Coulomb and exchange correction terms to the arithmetical mean of the HF orbital energies ϵ_a and ϵ_b. The corrections reflect the incorporation of both the occupied and the virtual orbital spaces by localizing hybridization. We computed a value of −0.311 au (−8.466 eV) for $\epsilon_\pm$ of C_2. This result is only 0.002 au (0.065 eV) more positive than the arithmetical mean of the $C_2(2\sigma_u)$ and $C_2(3\sigma_g)$ HF orbital energies.

From inspection of Table I, it is evident that all $C_2(^1\Sigma_g^+)$ and $N_2(^1\Sigma_g^+)$ MOs of σ type contribute remarkably to the building up of the delocalized 6σ MO of $CCNN(^1\Sigma^+)$. In the analysis of the 6σ MO, our predominant interest is to give an explanation of how the central CN bond of $CCNN(^1\Sigma^+)$ is constituted. The delocalized character of the $2\sigma_g$ MOs of both monomers is not altered by the process of bonding, and the charge density of these monomer MOs is for the most part located in the region of the terminal CC and NN bonds. This explains that the overlap of each $2\sigma_g$ MO with other σ orbitals in the central region of CCNN is found to be rather small. It follows that the $2\sigma_g$ MOs of $C_2(^1\Sigma_g^+)$ and $N_2(^1\Sigma_g^+)$ are of subordinate importance with respect to the formation of the central σ bond and thus to the stabilization of $CCNN(^1\Sigma^+)$ against unimolecular dissociation.

In Table I, it can be seen that the $2\sigma_u$ and $3\sigma_g$ MOs of $C_2(^1\Sigma_g^+)$ and $N_2(^1\Sigma_g^+)$ give a comparable contribution to the formation of the 6σ MO. This is strongly reminiscent of the constitution of the 9σ and 8σ MOs discussed above. The $2\sigma_u$ and $3\sigma_g$ MOs of $C_2(^1\Sigma_g^+)$ are found to exhibit a strong and binding overlap with the corresponding orbitals of $N_2(^1\Sigma_g^+)$ in the central region of $CCNN(^1\Sigma^+)$. Having in mind the localizing hybridization scheme, these results guide us to the only reasonable conclusion that the central σ bond of $CCNN(^1\Sigma^+)$ arises from the binding overlap of the localized hybrids of $C_2(^1\Sigma_g^+)$ and $N_2(^1\Sigma_g^+)$ that are directed toward the center of $CCNN(^1\Sigma^+)$. These localized hybrids represent the counterparts of those that constitute the 9σ and 8σ MOs.

Noting the pronounced minimum of the HF potential energy surface (Figure 1) of $CCNN(^1\Sigma^+)$, we find that the loss in the total HF energy (E_{LOC}; eq 8) due to localizing hybridization of $C_2(^1\Sigma_g^+)$ is clearly by far overcompensated by the gain in binding energy that is derived from the binding overlap of the centrally directed localized hybrids of $C_2(^1\Sigma_g^+)$ and $N_2(^1\Sigma_g^+)$. The stability of the $CCNN(^1\Sigma^+)$ system crucially depends on the fact that the four linearly combined monomer MOs that constitute the localized hybrids according to the localizing hybridization scheme are only occupied by six electrons (the $3\sigma_g$ MO of $C_2(^1\Sigma_g^+)$ is not occupied). This just represents the number of electrons necessary to doubly occupy the 6σ, 8σ, and 9σ MOs of $CCNN(^1\Sigma^+)$. If any further electron would be present in the $3\sigma_g$ MO of $C_2(^1\Sigma_g^+)$, it should necessarily promote to the virtual 10σ MO of $CCNN(^1\Sigma^+)$. The 10σ MO is the antibonding counterpart of the 6σ MO and lies at high energy (see Table I). Its occupation would lead to a partial or complete destabilization of $CCNN(^1\Sigma^+)$ as a whole. Of course, this conclusion applies to a linearly constrained $CCNN^-$ system, and it is conceivable that this molecule is stabilized by bending, as the case of the isoelectronic $(CO)_2^+$ system would suggest.[16]

It is reasonable to look upon both electrons of the $2\sigma_u$ MO of $C_2(^1\Sigma_g^+)$ as occupying the 9σ MO of $CCNN(^1\Sigma^+)$. Then, the centrally directed localized hybrid of $C_2(^1\Sigma_g^+)$ is empty, and according to the localizing hybridization scheme the central CN bond of $CCNN(^1\Sigma^+)$ represents a donative σ bond. This picture of the electronic constitution of the central CN bond is an obvious explanation for both the polarity of this bond (see Figure 2c) and the location of the positive center of partial charge at the central N atom of $CCNN(^1\Sigma^+)$ (see the valence structure given in section II).

IV. Beyond Hartree–Fock

In this section, we present the data obtained from variational single- and multiple-reference single- plus double-excitation configuration interaction computations (SDCI and MRCI, respectively).[17] In addition, we employed the modified coupled-pair

(17) Carsky, P.; Urban, M. Ab initio Calculations. *Lec. Notes Chem.* **1980**, *16* and references therein.

Table II. Calculated and Experimental Equilibrium Bond Lengths (Å) for CCNN, C_2, N_2, and CN[a]

bond	exptl	HF	SDCI	MRCI	MCPF
CCNN, *R*(CC)		1.248	1.266	1.275	1.288
CCNN, *R*(CN)		1.288	1.285	1.273	1.286
CCNN, *R*(NN)		1.109	1.118	1.130	1.143
C_2, *R*(CC)	1.243[b]	1.251	1.258		1.286
N_2, *R*(NN)	1.095[c]	1.078	1.106		1.117
CN, *R*(CN)	1.177[d]	1.114	1.136		

[a] Theoretical results were obtained with the DZP basis, and MRCI calculations employed a total of six CFs. [b] Reference 8. [c] Reference 9. [d] Reference 7.

function method (MCPF).[18] This is a nonvariational version of SDCI that corrects the size consistency error[19] of the latter. All computations were performed with the DZP basis (see section II). Due to the incorporation of electron correlation effects at the various CI levels, we expect a higher degree of accuracy and reliability with respect to the data we obtained at the HF level of theory.

Geometry. Table II comprises equilibrium structures of CCNN($^1\Sigma^+$) computed at HF and CI levels of theory. Additional data are given for the C_2, N_2, and CN molecules, which represent the units constituting the terminal and central bonds of CCNN. At CI level, each bond length was determined by fitting the computed potential energy to a parabola as a function solely of that length. The energy-minimizing bond length was carried on to the subsequent optimization of the other bond distances.

Inspecting Table II, we note an enlargement of the terminal bond distances in going from HF to SDCI or MCPF. On the other hand, the central CN bond distance is left almost completely unaltered. At MRCI level, the terminal bond lengths are between those computed at SDCI and MCPF levels and the central CN bond distance is strongly shortened by at least 0.01 Å. This would suggest that a rise in the incorporation of electron correlation effects increases the strength of the central CN bond. This results in a higher stabilization of CCNN($^1\Sigma^+$) as a whole. With respect to the structures of the CN, C_2, and N_2 molecules, it is evident from Table II that the central CN bond of CCNN($^1\Sigma^+$) is much more lengthened (0.096 Å in minimum) than the terminal CC (0.045 Å in maximum) and NN (0.048 Å in maximum) bonds. This clearly confirms our classification of CCNN($^1\Sigma^+$) as a codimer we proposed at HF level of theory (see section II).

Potential Energy Surfaces. Figure 5 illustrates the potential energy surfaces of CCNN($^1\Sigma^+$) computed at SDCI and MCPF levels of theory. The SDCI energies (curve A) were obtained with the optimized HF structures. However, the energy minimum is given at the SDCI-optimized geometry. Line B figures the total SDCI energy of the separated monomers $C_2(^1\Sigma_g^+)$ and $N_2(^1\Sigma_g^+)$ at their experimental geometries. Curve C and Line D represent the MCPF energies of CCNN($^1\Sigma^+$) and of the separated monomers, respectively, and have been computed with structures optimized at that level of theory.

The energetical separation between curves A and C or lines B and D is for the most part due to the correction of the size-consistency error of SDCI by the MCPF approach. Both methods confirm the (absolute) stability of CCNN($^1\Sigma^+$) to unimolecular dissociation into the constituent monomers $C_2(^1\Sigma_g^+)$ and $N_2(^1\Sigma_g^+)$. The binding energies of 1.03 eV at SDCI and 1.34 eV at the MCPF level are, however, remarkably reduced with respect to the HF result of 3.0 eV (see section II). This reduction of the binding energy is due to the incorporation of electron correlation effects at the CI levels and reflects the general tendency obtained in the series of molecules with empirical formula C_2N_2.[2] It is, however, important to note that the shapes of the SDCI and

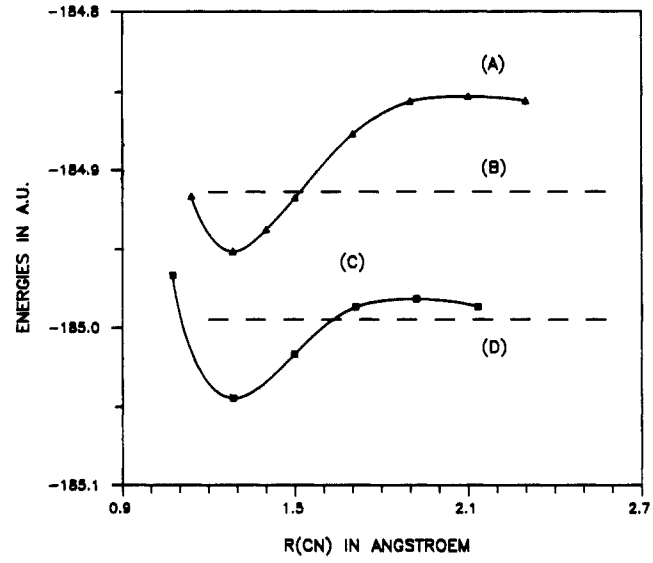

Figure 5. Potential energy surfaces of CCNN($^1\Sigma^+$) computed at SDCI (curve A) and MCPF (curve C) levels of theory. Lines B and D denote the total SDCI and MCPF energy of $C_2(^1\Sigma_g^+)$ and $N_2(^1\Sigma_g^+)$ at their experimental and optimized MCPF geometries, respectively. Energies were obtained with the DZP basis set.

MCPF energy surfaces confirm the existence of an energy barrier to unimolecular dissociation. Again, the height of the barrier is reduced to 2.69 eV at SDCI and 1.71 eV at MCPF level with respect to the value of 3.2 eV obtained with the HF method (see section II).

These results show that the minimal decrease of the binding energy due to the incorporation of electron correlation effects (1.66 eV) is larger than the maximal decrease of the energy barrier (1.49 eV). This tendency is even more expressed at the MRCI level of theory, which incorporates electron correlation effects to a larger extent than SDCI or MCPF. Our MRCI calculations indicate that both the equilibrium energy of CCNN($^1\Sigma^+$) and the total energy of the separated monomers $C_2(^1\Sigma_g^+)$ and $N_2(^1\Sigma_g^+)$ (representing the asymptotic limit) are strongly dependent on the number of configuration functions (CFs) used. As a general result, we found that the more CFs are incorporated the smaller becomes the binding energy. This behavior is only in part due to the size-consistency error of nonfull MRCI. It rather reflects the energy difference between the lowest unoccupied MO of CCNN($^1\Sigma^+$) ($\epsilon(3\pi^*)$ = +0.027 au (+0.073 eV)) and $C_2(^1\Sigma_g^+)$ ($\epsilon(3\sigma_g)$ = −0.11 au (−2.99 eV)). In this context, the analogous MO of the $N_2(^1\Sigma_g^+)$ molecule is of only subordinate importance. Because of the negative $3\sigma_g$ energy of the $C_2(^1\Sigma_g^+)$ molecule, the enlargement of the incorporation of electron correlation effects (i.e., increase in the number of CFs) lowers the energy of the asymptotic limit much more than the equilibrium energy of CCNN($^1\Sigma^+$). Therefore, we obtained binding energies of less than 0.1 eV at the MRCI level (our best calculations incorporated about 10 CFs for CCNN($^1\Sigma^+$), $C_2(^1\Sigma_g^+)$, and $N_2(^1\Sigma_g^+)$). Since our MRCI calculations are rather limited in the number of CFs and unbalanced with respect to the incorporation of electron correlation effects at CCNN($^1\Sigma^+$) and especially at $C_2(^1\Sigma_g^+)$, we are not yet able to give a definite statement about whether CCNN($^1\Sigma^+$) is absolutely stable to unimolecular dissociation into the closed-shell monomers $C_2(^1\Sigma_g^+)$ and $N_2(^1\Sigma_g^+)$. However, the MRCI calculations clearly confirm that the energy barrier to unimolecular dissociation should stay with a remarkable height (about 2 eV as a reasonable estimate based on our MRCI data).

To conclude, we state that our HF, SDCI, and MCPF calculations clearly confirm the stability of CCNN($^1\Sigma^+$) to unimolecular dissociation while the MRCI computations only allow us to state unequivocally that CCNN($^1\Sigma^+$) should be at least metastable (kinetically stabilized) to dissociation because of the existence of a remarkable energy barrier. It would be desirable to carry out more sophisticated calculations with larger basis sets

(18) Chong, D. P.; Langhoff, S. R. *J. Chem. Phys.* **1986**, *84*, 5606. Ahlrichs, R.; Scharf, P.; Ehrhardt, C. *J. Chem. Phys.* **1985**, *82*, 890. We thank M. Rosi for helpful discussions and C. W. Bauschlicher for making available his MCPF program.

(19) Wilson, S. *Electron Correlation in Molecules*; Clarendon Press: Oxford, 1984.

to substantiate the above interesting findings.

V. Conclusions

A first theoretical analysis of CCNN, the fourth and last possible isomer with empirical formula C_2N_2, was presented in this work. At Hartree–Fock and various configuration interaction levels of theory a closed-shell ground state $^1\Sigma^+$ and a linear equilibrium geometry were confirmed. Chemical bonding was found to occur between the closed-shell monomers $C_2(^1\Sigma_g^+)$ and $N_2(^1\Sigma_g^+)$. $CCNN(^1\Sigma^+)$ must thus be classified as a normal molecule in a chemical sense, and the possible model of a van der Waals complex can be excluded unequivocally. At Hartree–Fock level, the analysis of the charge density distribution revealed a new type of binding mechanism, referred to as localizing hybridization. At all levels of calculations presented in this work, the existence of an energy barrier to unimolecular dissociation into the closed-shell monomers $C_2(^1\Sigma_g^+)$ and $N_2(^1\Sigma_g^+)$ was confirmed. The appearance of the energy barrier reflects the loss in the total energy of $CCNN(^1\Sigma^+)$ due to localizing hybridization of the $C_2(^1\Sigma_g^+)$ monomer. While the kinetical stabilization of $CCNN(^1\Sigma^+)$ is assured, we are not yet able to give a definitive statement about whether the system is also absolutely stable to unimolecular dissociation into the closed-shell monomers $C_2(^1\Sigma_g^+)$ and $N_2(^1\Sigma_g^+)$. For the most part, this uncertainty depends on the only partial incorporation of the strong electron correlation effects present at the $C_2(^1\Sigma_g^+)$ monomer. We stress that large-scale configuration interaction computations or methods of equivalent accuracy with larger basis sets should be very helpful to clarify the interesting question about whether $CCNN(^1\Sigma^+)$ is absolutely or kinetically stable to unimolecular dissociation.

We assume the $CCNN(^1\Sigma^+)$ system to be fairly reactive and to exhibit unusual chemical and physical properties. The large dipole moment, which is strongly varying with the central CN bond length of CCNN (distance between the monomers C_2 and N_2), is of particular interest. The (absolutely or kinetically) stable chemical bonding of the closed-shell molecules $C_2(^1\Sigma_g^+)$ and $N_2(^1\Sigma_g^+)$ should be of potential interest for further theoretical and experimental investigations. As an outlook, we focus the readers' attention on the $CCCO(^1\Sigma^+)$ molecule, the monomers of which are isoelectronic to those of CCNN. Investigations are in progress that indicate that the stability of the codimer $CCCO(^1\Sigma^+)$ to unimolecular dissociation depends on a binding mechanism essentially identical with the localizing hybridization scheme introduced in this work. A further interesting question may be whether the astrophysical importance of CCCO is also valid for the CCNN system.

Photochemical Ligand Loss as a Basis for Imaging and Microstructure Formation in a Thin Polymeric Film

Sharon Gould, Terrence R. O'Toole, and Thomas J. Meyer*

Contribution from the Kenan Laboratories of Chemistry, University of North Carolina, Chapel Hill, North Carolina 27599-3290. *Received May 21, 1990*

Abstract: Ligand loss photochemistry occurs in thin polymeric films of poly$[Ru(bpy)_2(vpy)_2]^{2+}$ (bpy is 2,2′-bipyridine, vpy is 4-vinylpyridine), poly$[Ru(Me_2bpy)_2(vpy)_2]^{2+}$ (Me_2bpy is 4,4′-dimethyl-2,2′-bipyridine), and poly$[Ru(Me_4bpy)_2(vpy)_2]^{2+}$ (Me_4bpy is 4,4′,5,5′-tetramethyl-2,2′-bipyridine). These films were formed by reductive electropolymerization of the corresponding 4-vinylpyridine complexes on Pt disk electrodes. Upon photolysis, the ruthenium–pyridyl bonds were cleaved and the polymer was lost, exposing the underlying substrate. The photochemical reaction was used to transfer an image to the films by using masking techniques. In a subsequent step, poly$[Os(vbpy)_3]^{2+}$ (vbpy is 4-methyl-4′-vinyl-2,2′-bipyridine), which is photochemically stable, was formed selectively in the exposed regions of the electrode by reductive electropolymerization. This procedure gave a laterally resolved, two-component, film-based structure in which there were discrete, spatially segregated regions of Ru^{II} and Os^{II}. In a final step, the remaining film containing Ru^{II} was removed by photolysis. This procedure left an image of the original mask in the poly$[Os(vbpy)_3]^{2+}$ that remained.

Introduction

Thin films of polymeric, polypyridyl complexes of Ru^{II}, Os^{II}, or Re^{I} can be prepared by well-established synthetic procedures that are based on electropolymerization on conductive substrates.[1] It has been shown that in these films the individual metal complex sites retain, to a high degree, the oxidation–reduction, light absorbance, and even reactivity characteristics of related complexes in solution. The synthetic chemistry based on electropolymerization is well developed, with procedures available for preparing multicomponent films or multilayer structures in which different components are separated in distinct layers. Even given the rapid evolution of this chemistry, an outstanding problem that remains to be solved is how to build spatially controlled, vertical structures that are perpendicular to the underlying substrate.

The photochemistry of the polypyridyl complexes in solution is well-defined and extensive.[2] It includes examples of photochemical energy conversion based on electron transfer and studies of intramolecular electron or energy transfer in complex molecular assemblies.

The photochemical reactivity also exists for individual metal-complex sites in thin polymeric films. Examples are known

(1) (a) Calvert, J. M.; Schmehl, R. H.; Sullivan B. P.; Facci, J. S.; Meyer, T. J.; Murray, R. W. *Inorg. Chem.* **1983**, *22*, 2151. (b) Denisevich, P.; Abruña, H. D.; Leidner, C. R.; Meyer, T. J.; Murray, R. W. *Inorg. Chem.* **1982**, *21*, 2153–2161. (c) Murray, R. W. *Annu. Rev. Mater. Sci.* **1984**, *14*, 145–169. (d) O'Toole, T. R.; Margerum, L. D.; Bruce, M. R.; Sullivan, B. P.; Murray, R. W.; Meyer, T. J. *J. ELectroanal. Chem. Interfacial Electrochem.* **1989**, *259*, 217–238. (e) Deronzier, A.; Moutet, J.-C. *Acc. Chem. Res.* **1989**, *22*, 249–255.

(2) (a) Juris, A.; Balzani, V.; Barigelletti, F.; Campagna, S.; Belser, P.; Von Zelewsky, A. *Coord. Chem. Rev.* **1988**, *84*, 85. (b) Kalyanasundaram, K. *Coord. Chem. Rev.* **1982**, *46*, 159. (c) Whitten, D. G. *Acc. Chem. Res.* **1980**, *13*, 83. (d) Sutin, N.; Creutz, C. *Pure Appl. Chem.* **1980**, *52*, 2717. (e) Watts, R. J. *J. Chem. Educ.* **1983**, *60*, 834. (f) Meyer, T. J. *Pure Appl. Chem.* **1986**, *58*, 1193. (g) Ferguson, J.; Herren, F.; Krausz, E.; Vrbancich, J. *Coord. Chem. Rev.* **1985**, *64*, 21. (h) Meyer, T. J. In *Progress in Inorganic Chemistry*; Lippard, S. J., Ed.; Wiley & Sons: New York, 1983, Vol. 30, p 389. (i) Meyer, T. J. *Acc. Chem. Res.* **1989**, *22*, 163.

0002-7863/90/1512-9490$02.50/0